Journal of Advances in Physical Chemistry 物理化学进展, 2024, 13(3), 508-522
Published Online August 2024 in Hans. https://www.hanspub.org/journal/japc
https://doi.org/10.12677/japc.2024.133055

Hans汉斯

镍－稀土单分子磁体的研究进展

李晴燕[1]，李　佳[1]，刘　雨[1]，胡翔宇[1]，崔会会[1]，朱金丽[1]，王　金[1]，丁欣宇[1,2*]

[1]南通大学化学化工学院，江苏　南通
[2]南通智能与新能源材料重点实验室，江苏　南通

收稿日期：2024年7月17日；录用日期：2024年8月20日；发布日期：2024年8月29日

摘　要

镍(II)离子具有3d[8]的电子构型。在八面体场中，它们倾向于采用高自旋，表现为顺磁性，而在正方形平面场中，它们通常采用低自旋，表现为抗磁性。镍(II)可以与具有f[7]-f[11]电子构型的镧系离子进行铁磁耦合，如镝(III)。镍(II)离子内的二阶轨道角动量可以提供大量的零场分裂参数，这意味着可能存在显著的磁各向异性。因此，本文通过对近年来典型的镍－稀土单分子磁体进行综述，以期为3d-4f单分子磁体的发展奠定一定的基础。

关键词

镍－稀土单分子磁体，结构，磁性

Research Progress in Ni-Ln SMMs Single Molecule Magnets

Qingyan Li[1], Jia Li[1], Yu Liu[1], Xiangyu Hu[1], Huihui Cui[1], Jinli Zhu[1], Jin Wang[1], Xinyu Ding[1,2*]

[1]School of Chemistry and Chemical Engineering, Nantong University, Nantong Jiangsu
[2]Nantong Key Laboratory of Intelligent and New Energy Materials and Devices, Nantong Jiangsu

Received: Jul. 17th, 2024; accepted: Aug. 20th, 2024; published: Aug. 29th, 2024

Abstract

Nickel(II) ions possess electronic configuration of 3d[8]. In an octahedral field, they tend to adopt a high-spin, exhibiting paramagnetism, whereas in a square-planar field, they typically adopt a low-spin, manifesting as diamagnetism. Ni(II)can engage in ferromagnetic coupling with lanthanide ions having electronic configurations of f7-f11, such as dysprosium(III). Additionally, the second-order or-

*通讯作者 Email: ding.xyu@ntu.edu.cn

文章引用: 李晴燕, 李佳, 刘雨, 胡翔宇, 崔会会, 朱金丽, 王金, 丁欣宇. 镍-稀土单分子磁体的研究进展[J]. 物理化学进展, 2024, 13(3): 508-522. DOI: 10.12677/japc.2024.133055

bital angular momentum within Nickel(II) ions can provide substantial zero-field splitting parameters, implying the potential for significant magnetic anisotropy. Therefore, this paper reviews the typical nickel-rare earth single molecule magnets in recent years, in order to lay a certain foundation for the development of 3d-4f single molecule magnets.

Keywords

Ni-Ln Single Molecule Magnets, Structure, Magnetism

1. 引言

单分子磁体(Single-Molecule Magnets, SMMs)是一类有机分子纳米磁体，晶格中分子间距远，分子间相互作用很弱，晶体的整体性质可以看做全同分子性质的叠加。它的出现使得以纳米尺度磁性配合物作为基本单元研制存储器件成为可能。SMMs 在二十年来的广泛关注，主要是因为其在分子水平或纳米尺度的高密度信息存储方面的潜在应用[1]-[4]。

1993 年，Sessoli R.首次报道了由 12 个 Mn 离子[$Mn_{12}O_{12}(OCMe)_{16}(H_2O)_4$] ($Mn_{12}$-ac)组成的金属团簇在低温下具有类似于磁畴的单分子超顺磁性[5]，从而开启了单分子磁体的研究领域。早期阶段，研究主要围绕 3d 过渡金属离子展开，特别是 Mn 基单分子磁体，希望通过提高配合物分子内金属离子的数目以提高分子的总基态自旋值，从而增强单分子磁体的慢磁弛豫性能。单分子磁体的发展大致经历了三个阶段：nd-SMMs [10]-[12]、nd-nf-SMMs [10]-[12]和 nf-SMMs [13]-[16]。

近年来，具有独特电子结构的镧系离子因其无与伦比的单离子各向异性而引起了人们的广泛关注。最显著的重镧系离子，如 Dy^{III}、Tb^{III}、Ho^{III} 和 Er^{III}，已被广泛用作构建 SMMs 的磁性中心。自第一个铁磁 Cu^{II}-Gd^{III} 化合物被报道后[11]，3d-4f 杂金属复合物吸引了大量的兴趣，因为他们是有效的模型化合物在理解 3d 和 4f 之间的磁交换金属离子，特别是一些 3d-4f 集群作为 SMMs。3d 和 4f 离子之间的强磁相互作用使其更容易显示 SMM 行为。三维金属离子主要包括 Cu^{II}、Ni^{II}、Co^{II} 和 Mn^{III} 离子，通常选择多齿状席夫碱配体来构建 3d-4f 异金属 SMMs [17]。由镧系金属与有机配体形成的多功能配合物在许多领域表现出了其特殊的应用价值[18] [19]。首先，因为 Ln (III)离子具有强大的自旋－轨道耦合和较大的磁各向异性，成为开发高性能单分子磁体(SMMs)的首选目标，这些固有的磁特性使得 Ln-SMMs 在高密度信息存储、量子处理、磁性制冷、自旋电子学等方面具有潜在的应用；其次，由于稀土离子本身的独特结构和性质，使其与合适的有机配体结合后，所发出的荧光兼有稀土离子发光强度高、颜色纯正和有机化合物所需激发能量低、发光效率高等优点[20] [21]。

然而，实现基于 SMM 的存储技术还存在两个主要问题，一个是 SMMs 的缓慢磁弛豫的温度，另一个是由于 SMMs 的单个分子，难以沉积和处理在表面[22]上，存储设备的制造遇到了很大的困难。因此，研究分子基磁体的一大挑战之一仍然是设计和合成高效的 SMMs。本文按照镍－稀土单分子磁体的性质类型进行综述，总结了关于镍－稀土单分子磁体研究进展的相关报道，以期望能开发高性能的 SMMs。

2. 镍－稀土单分子磁体的研究进展

目前，已报道的镍－稀土单分子磁体如表 1 所示，本论文仅选其中一些例子进行描述，并根据其核

数进行分类，以研究其结构与磁性行为之间的关系。

Table 1. The magnetic data of Ni-Ln SMMs
表 1. 镍－稀土单分子磁体的磁性数据

Complexes	H_{dc}/k Oe	U_{eff}/K	τ_0/s	v/m T/s	T_B /K	Ref.
$[Dy_2Ni_2L^1(bipy)_2]$ (**1**)	0	105(1)	1.85×10^{-11}			[23]
$[Dy_2Ni(C_7H_5O_2)_8]\cdot(C_7H_6O_2)_2$ (**2**)	1.5	55.19	5.21×10^{-8}			[24]
$[Dy_2Ni_2(bipy)_2(HC_6H_5COO)_{10}]$ (**3**)	0	57.06	1.80×10^{-8}			[25]
$[Dy_2Ni_2(bipy)_2(CH_3C_6H_4COO)_{10}]$ (**4**)	0	37.04	1.16×10^{-6}			[25]
$[Dy_2Ni_2(bipy)_2(NO_3C_6H_4COO)_{10}]$ (**5**)	0	4.0	5.47×10^{-6}			[25]
$[Ni_2Dy_2(L^2)_4(NO_3)_2(DMF)_2]$ (**6**)	0	18.5	5.4×10^{-7}	140	1.1	[26]
$[Ni_2Dy_2(L^2)_4(NO_3)_2(MeOH)_2]\cdot 3MeOH$ (**8**)	0	21.3	1.5×10^{-6}			[26]
$[Tb_2Ni_4(L^3)_2Cl_2(OH)_2(CH_3O)_2(CH_3OH)_6]$ (**11**)	0	30	2.09×10^{-9}			[27]
$[Dy_2Ni_4(L^3)_2Cl_2(OH)_2(CH_3O)_2(CH_3OH)_6]$ (**12**)	0	32	1.41×10^{-8}			[27]
$[Dy_2Ni_2(H_2L^5)_2(\mu_3\text{-}OMe)_2(CH_3CN)_2(NO_3)_4]\cdot 4H_2O$ (**15**)	0	48.2	3.6×10^{-8}			[28]
$[Tb_2Ni_2(HL^4)_2(\mu_3\text{-}OMe)_2(CH_3CN)_2(NO_3)_4]\cdot 4H_2O$ (**16**)	0	86.2	2.3×10^{-7}			[28]
$[Dy_2Ni_2(HL^4)_2(\mu_3\text{-}OMe)_2(CH_3CN)_2(NO_3)_4]\cdot 4H_2O$ (**17**)	0	56.6	3.3×10^{-8}			[28]
$[Ni_2Dy_3(HL^6)_4]Cl$ (**18**)	0	$U_1 = 53.5$ $U_2 = 85$	$\tau_1 = 2.3 \times 10^{-8}$ $\tau_2 = 5.9 \times 10^{-7}$	50	3	[29]
$[Ni_6Dy_3(OH)_6(HL^7)_6(NO_3)_3]\cdot 2MeCN\cdot 2.7Et_2O\cdot 2.4H_2O$ (**23**)	0	23.84	3.63×10^{-8}			[30]
$[HoNi_5(quinha)_5F_2(dfpy)_{10}]$ (**25**)	0	$U_1 = 32.7$ $U_2 = 825.1$	$\tau_1 = 9.4(2) \times 10^{-4}$ $\tau_2 = 3.3(5) \times 10^{-13}$	20	4	[32]
$[Ni_4Dy_2(CO_3)_2Cl_2(L^8)_2(L^9)_2(CH_3CN)_2]\cdot 4CH_3CN\cdot 2H_2O$ (**26**)	2	43(7)	3×10^{-12}			[32]
$[\{Dy(hfac)_3\}_2\{Ni(bpca)_2\}]\cdot CHCl_3$	1	4.9	$1.3(0.2) \times 10^{-6}$			[33]
$[(L^{10})_2Ni_2Dy][ClO_4]$	3.5	10.8	2.3×10^{-5}			[34]
$[\{L^{Me2}Ni(H_2O)Tb(dmf)_{2.5}(H_2O)_{1.5}\}\{W(CN)_8\}]\cdot H_2O\cdot 0.5dmf$	0	15.3	4.5×10^{-7}			[35]
$[Ni(\mu\text{-}L^{11})(\mu\text{-}NO_3)Dy(NO_3)_2]_3\cdot 2CH_3OH$	1	19.1	7.2×10^{-7}			[36]
$[Dy_2Ni_2(\mu_3\text{-}OH)_2(OH)(OAc)_4(HL^{12})_2(MeOH)_3](ClO_4)\cdot 3MeOH$	1.2	7.6	7.5×10^{-6}			[37]
$[Ni(\mu\text{-}L^{11})(\mu\text{-}OBz)Dy(NO_3)_2]\cdot CH_3OH$	1	9.2	4.4×10^{-6}			[38]
$[Ni(\mu\text{-}L^{11})(\mu\text{-}9\text{-}An)Dy(9\text{-}An)(NO_3)_2]\cdot 3CH_3CN$	1	10.1	3.4×10^{-6}			[38]
$[Dy_{42}Ni_{10}(\mu_3\text{-}OH)_{68}(CO_3)_{12}(CH_3COO)_{30}(H_2O)_{70}]\cdot(ClO_4)_{24}\cdot 80H_2O$	0	3.43	1.27×10^{-6}			[39]
$[(\mu_4\text{-}CO_3)_2\{Ni(3\text{-}MeOsaltn)(MeOH)Tb(NO_3)\}_2]$	1	12.2(7)	$4.6(11) \times 10^{-7}$			[40]
$[(\mu_4\text{-}CO_3)_2\{Ni(3\text{-}MeOsaltn)(MeOH)Dy(NO_3)\}_2]$	0 1	6.6(4) 18.1(6)	$1.6(3) \times 10^{-6}$ $1.8(4) \times 10^{-7}$			[40]
$[(\mu_4\text{-}CO_3)_2\{Ni(3\text{-}MeOsaltn)(H_2O)Tb(NO_3)\}_2]\cdot 2CH_3CN\cdot 2H_2O$	1	6.1(3)	$9.7(15) \times 10^{-7}$			[40]
$[(\mu_4\text{-}CO_3)_2\{Ni(3\text{-}MeOsaltn)(H_2O)Dy(NO_3)\}_2]\cdot 2CH_3CN\cdot 2H_2O$	1	14.5(4)	$4.2(8) \times 10^{-8}$			[40]
$[Ni(3\text{-}MeOsaltn)(MeOH)_x(ac)Tb(hfac)_2]$	1	14.9(6)	$2.1(5) \times 10^{-7}$			[41]
$[Ni_2Dy_2(CH_3CO_2)_3(HL^{13})_4(H_2O)_2](NO_3)_3$	0	19	4.23×10^{-7}			[42]
$[Ni_3Dy_3(\mu_3\text{-}O)(\mu_3\text{-}OH)_3(L^{14})_3(\mu\text{-}OOCCMe_3)_3]$	3	10	10^{-6}			[43]
$[Ni_2Dy_2(\mu_3\text{-}OH)_2(O_2C^tBu)_{10}[Et_3NH]_2]$	0	20	6.0×10^{-7}			[44]
$[Ni_2Er_2(\mu_3\text{-}OH)_2(O_2C^tBu)_{10}[Et_3NH]_2]$	1	18	3.9×10^{-6}			[44]

续表

$\{[NH_2(CH_3)_2]_2[NiDy_2(HCOO)_2(abtc)_2]\}_n$	1	42	4.7×10^{-6}			[45]
$\{[Ni(Me_2valpn)]_2Dy(H_2O)Cr(CN)_6\}_2 \cdot 14H_2O \cdot 2DMF$	0	38.9	4.89×10^{-9}			[46]
$\{[Ni(Me_2valpn)]_2Dy(H_2O)Cr(CN)_6\}_2 \cdot 24H_2O \cdot 2PPPO \cdot 2CH_3CN$	0	37.2	6.44×10^{-9}			[46]
$\{[Ni(Me_2valpn)]_2Dy(H_2O)Co(CN)_6\}_2 \cdot 8H_2O \cdot 2DMF \cdot 6CH_3CN$	0	24.4	4.94×10^{-7}			[46]
$\{[Ni(Me_2valpn)]_2Tb(H_2O)Cr(CN)_6\}_2 \cdot 12H_2O \cdot 3DMF$	0	21.9	4.71×10^{-8}			[46]
$\{[Ni(Me_2valpn)]_2Tb(H_2O)Fe(CN)_6\}_2 \cdot 13.31H_2O \cdot 2DMF \cdot 2.69CH_3CN$	0	29.6	4.52×10^{-10}			[46]
$[Ni_2Dy_2(Hhms)_2(CH_3COO)_6(CH_3OH)_2(H_2O)_2] \cdot (NO_3)_2$	0	16.9	6.5×10^{-7}			[47]
$[Ni_6Dy(L^{15})_4(Htea)_4](ClO_4)_{2.5}(NO_3)_{0.5} \cdot 5.5MeCN \cdot H_2O$	0	10	1.5×10^{-5}			[48]
$[Dy_{45}Ni_7(OH)_{68}(CO_3)_{12}(CH_3COO)_{26}(CH_3CH_2COO)_6(H_2O)_{70}]$	0	3.42	9.25×10^{-7}			[49]
$[Ni_2Dy_2(L^{16})_4(NO_3)_2(H2O)_2] \cdot 2H_2O$	0	35.75	8×10^{-8}			[50]
$[Ni_4Dy_2(\mu_3\text{-}OH)_2(L^{17})_4(OAc)_8] \cdot H_2O$	0	11.2(2)	$8.9(6) \times 10^{-6}$			[51]
$[Ni_4Dy_2(L^{18})_2(\mu\text{-}Cl)_2(\mu_3\text{-}OH)_4(H_2O)_6]Cl_4 \cdot 2H_2O$	0	23.0	4.52×10^{-9}			[52]
$[Ni_4Tb_2(L^{18})_2(\mu\text{-}Cl)_2(\mu_3\text{-}OH)_4(H_2O)_6]Cl_4 \cdot 2H_2O$	0	26.3	1.07×10^{-9}			[52]
$[Ni_4Dy_2(L^{18})_2(\mu\text{-}NCS)_2(\mu_3\text{-}OH)_4(NCS)_4(H_2O)_2] \cdot 2MeOH \cdot 4H_2O$	0	26.0	1.56×10^{-8}			[52]
$[Ni_4Tb_2(L^{18})_2(\mu\text{-}NCS)_2(\mu_3\text{-}OH)_4(NCS)_4(H_2O)_2] \cdot 14.1H_2O$	0	30.6	5.03×10^{-9}			[52]
$[NiDy(L^{19})(Pc)(CH_3OH)] \cdot CH_3OH$	1	6.2				[53]
$[NiCe(L^{20})(NO_3)_3]$	0.5	8.5	7.7×10^{-5}			[54]
$[NiNd(L^{20})(NO_3)_3]$	1	9.2	1.9×10^{-5}			[54]
$[NiDy(L^{20})(NO_3)_3]$	1	9.3	2.1×10^{-5}			[54]
$[NiEr(L^{20})(NO_3)_3]$	1	18.4	1.7×10^{-6}			[54]
$[NiYb(L^{20})(NO_3)_3]$	1	18.1	2.1×10^{-6}			[54]
$[Ni_2Dy_2(L^{21})_2(CH_3CN)_3(H_2O)(NO_3)_6] \cdot (CH_3CN)_2 \cdot (H_2O)$	1	19	1.6×10^{-8}			[55]
$[Ni_2Dy_2(L^{22})_2(CH_3CN)_4(NO_3)_6] \cdot (CH_3CN)_x$	1	15.9	2.6×10^{-7}			[55]
$[Dy_2Ni_2(3, 4\text{-}DCB)_{10}(2, 2'\text{-}bpy)_2]$	2	7.0	6.8×10^{-5}			[56]
$[Ni(L^{23})Dy(H_2O)_4][Co(CN)_6] \cdot 3H_2O$	0.8	47.02	6.7×10^{-9}			[57]
$[Dy_2Ni_4(L^{24})_4(\mu_{1,3}\text{-}CH_3CO_2)_2(\mu_3\text{-}OH)_4(MeOH)_2] \cdot 4CH_3OH$	0	13.4(5)	$3.4(2) \times 10^{-7}$	60	0.7	[58]
$[Dy_2Ni_2Mn_2(L^{24})4(\mu_{1,3}\text{-}CH_3CO_2)_2(\mu_3\text{-}OH)_4(MeOH)_2](NO_3)_2 \cdot 2CH_3OH$	0	13.0(5)	$2.8(5) \times 10^{-7}$			[58]
$[\{(NiL^{25})_2Tb\}_2(\mu_2\text{-}Cl)_2Cl_2(\mu_3\text{-}OH)_4(OH_2)_2]Cl_2 \cdot 12H_2O$	0	13.3(5)	$3.8(8) \times 10^{-9}$			[59]
$[\{(NiL^{25})_2Dy\}_2(\mu_2\text{-}Cl)_2Cl_2(\mu_3\text{-}OH)_4(OH_2)_2]Cl_2 \cdot 16H_2O$	0	$U_1 = 19.4(8)$ $U_2 = 19.8(3)$	$\tau_1 = 5(1) \times 10^{-11}$ $\tau_2 = 9(1) \times 10^{-10}$			[59]
$[\{(NiL^{25})_2Ho\}_2(\mu_2\text{-}Cl)_2(\mu_3\text{-}OH)_4(OH_2)_4]Cl_4 \cdot CH_3CN \cdot 1.8H_2O$	0	$U_1 = 19.8(8)$ $U_2 = 18.5(6)$	$\tau_1 = 1.6(5) \times 10^{-10}$ $\tau_2 = 2.4(5) \times 10^{-9}$			[59]
$[Ni_4Dy(L^{26})_2(LH)_2(CH_3CN)_3Cl] \cdot 5H_2O \cdot CH_3OH$	4	35.9	4.36×10^{-9}			[60]
$[Ni_4Er(L^{26})_2(LH)_2(CH_3CN)_3Cl] \cdot 2H_2O \cdot 2CH_3OH$	4	31.6	7.94×10^{-11}			[60]
$[Ni_2Dy(EtOH)(L^{27})_4(NO_3)_2Cl] \cdot CH_3CN$	3	9.48	2.25×10^{-6}			[61]
$[NiDy(L^{28})(dca)_2(NO_3)]_n$	1	26.2(5)	$2.8(4) \times 10^{-7}$			[62]
$[Tb(hfac)_3Ni(hfac)_2NIT\text{-}4py(H_2O)_2]$	0	7.0	7.8×10^{-7}			[63]
$[Dy_2Ni_4(L^{29})_8(CH_3COO)_4(NO_3)_2]$	0	7.43	9.19×10^{-7}			[64]
$[Dy_4Ni_8(\mu_3\text{-}OH)_8(L^{30})_8(OAc)_4(H_2O)_4] \cdot 3.5EtOH \cdot 0.5CH_3CN \cdot 5H_2O$	0	7.66	1.45×10^{-6}			[65]
$[Ni_2(valpn)_2Dy_2(DMF)_5(H_2O)][Fe(1\text{-}CH_3im)(CN)_5]_3 \cdot 4DMF \cdot 12H_2O$	0	14.8(3)	$1.4(9) \times 10^{-6}$			[66]

续表

$[Dy_2Ni_2(2, 3\text{-DCB})_{10}(2, 2'\text{-bpy})_2]$	2	4.4	3×10^{-5}		[67]
$[Dy_4Ni_8(\mu_3\text{-OH})_8(L^{31})_8(OAc)_4(H_2O)_4]\cdot 3.25EtOH\cdot 4CH_3CN$	1	81.14(3)	$6.21(2) \times 10^{-11}$	2	[68]
$[Gd_2Ni_3(dto)_6(H_2O)_{10}]\cdot 12H_2O$	2.5	22.7	$1.54(5) \times 10^{-6}$		[69]
$[Gd_2Ni_3(dto)_6(H_2O)_{10}]\cdot 2H_2O$	2.5	18.33	$3.25(5) \times 10^{-6}$		[69]
$[NiEr(L^{32})_2(NO_3)_3]\cdot 0.5H_2O$	1	12.1(2)	$3.49(2) \times 10^{-7}$		[70]
$[NiDy(H_2L^{33})(NO_3)_3]\cdot(CH_3OH)_2$	0.6	17.01	4.09×10^{-8}		[71]
$[Ni_2Dy_2(L^{34})_4(Ac)_2(DMF)_2]\cdot 3CH_3CN$	0	18	6.85×10^{-6}		[72]
$[Ni_2Dy(Hhmmp)_2\{(py)_2CO_2\}(CH_3COO)_2]OH$	0	6.44	1.29×10^{-7}		[73]
$[Ni_2Dy(TTTT^{Me})_2(DMF)]BPh_4$	0	582	$1.4(4) \times 10^{-11}$		[74]
	0.3	582	$1.3(4) \times 10^{-11}$		[74]
$[Dy_2Ni_2(2, 5\text{-DCB})_{10}(phen)_2]$	2	10	4.0×10^{-5}		[75]

HL^1 = 3, 5-dichlorobenzoic acid; bipy = 2, 2'-bipyridine; $C_7H_6O_2$ = salicylic aldehyde; H_2L^2 = (E)-2-(2-Hydroxy-3-methoxybenzylideneamino)phenol; H_2L^3 = N1, N3-bis(3-methoxy-salicylidene)-diethylenetriamine; H_3L^4 = 2-(2, 3-dihydroxpropyliminomethyl)-6-methoxyphenol; H_4L^5 = 2-(((2-hydroxy-3-methoxyphenyl)methylene)amino)-2-(hydroxymethyl)-1, 3-propanedio; H_4L^6 = (E)-2, 2'-(2-hydroxy-3-((2-hydroxyphenylimino)methyl)-5-methylbenzylazanediyl)diethanol; H_3L^7 = 2-(*β*-naphthalideneamino)-2-hydroxymethyl-1-propanol; H_2quinha = quinaldichydroxamic acid, dfpy = 3, 5-difluoropyridine; H_2L^8 = N-salicylidene-N'-3-methoxysalicylidene-1, 3-propanediamine; H_2L^9 = N, N'-bis(salicylidene)-1, 3-propanediamine; $hfac^-$ =1, 1, 1, 5, 5, 5-hexafluoroacetylacetonate; $bpca^-$ =bis(2-pyridylcarbonyl)amine anion; L^{10} = (S)P[N(Me)N=CH-C_6H_3-2-O-3-OMe]$_3$; Hdpk = di-2-pyridyl ketoxime; L^{Me2} = 6, 6'-((1E, 1'E)-((2, 2-dimethylpropane-1, 3-diyl)bis(azaneylylidene))bis(methaneylylidene))bis(2-methoxyphenol); dmf = dimethylformamide; H_2L^{11} = N, N', N"-trimethyl-N, N"-bis(2-hydroxy-3-methoxy-5-methylbenzyl)diethylenetriamine; H_2L^{12} = 2-(benzothiazol-2-ylhydrazonomethyl)-6-methoxyphenol; OBz = benzoate; 9-An = 9-antharecenecarboxylate; 3-MeOsaltn = N, N'-bis(3-methoxy-2-oxybenzylidene)-1, 3-propanediaminato; HL^{13} = 2-methoxy-6-[(E)-2'-hydroxymethyl-phenyliminomethyl]-phenolate; H_2L^{14} = 6, 6'-{(2-(dimethylamino)-ethylazanediyl)bis(methylene)}bis(2-methoxy-4-methylphenol); H_4abtc = 3, 3', 5, 5'-azobenzene-tetracarboxylic acid; H_2Me$_2$valpn = N, N'-bis(3-methoxysalicylidene)-2, 2-dimethyl-1, 3-diaminopropane); H_2hms = 1-(2-hydroxy-3-methoxybenzylidene)-semicarbazide; H_3tea = triethanolamine; HL^{15} = 11H-indeno[1, 2-b]quinoxalin-11-one ligand; H_2L^{16} = 3-ethoxysalicylaldehyde with 2-aminophenol; HL^{17} = 1, 3-diamine-2-propanol; H_2L^{18} = 2-((2-(2-(2-hydroxy-3-methoxybenzylideneamino)ethylthio)ethylimino)methyl)-6-methoxyphenol); H_3L^{19} = 1, 1, 1-tris[(salicylideneamino)methyl]ethane; H_2Pc = phthalocyanine; H_2L^{20} = (*RR*)/(SS)-1, 2-diphenyl-ethylenediamine with o-vanillin; H_2L^{21} = N, N-bis(2-hydroxy-3-methoxy-benzyliden)-1, 4- diaminobenzene; H_2L^{22} = N, N-bis(2-hydroxy-3-methoxy-benzyliden)-1, 5-diaminonaphthalene; 3, 4-HDCB = 3, 4-dichlorobenzoic acid; H_2L^{23} = N, N-ethylenebis(3-methoxysalicylaldiimine); H_2L^{24} = 2-{[(2-hydroxy-3-methoxybenzyl)imino]methyl}phenol; HL^{25} = 2-((3-aminopropylimino)methyl)-6-methoxyphenol; H_3L^{26} = (E)-2-(hydroxymethyl)-6-(((2-hydroxyphenyl)imino)methyl)-4-methylphenol; HL^{27} = 2-methyl-8-hydroxyquinoline; H_2L^{28} = N, N'-bis(2-hydroxy-3-methoxy-5-methylbenzyl)homopiperazine; dca = dicyanamide; hfac = hexafluoroacety-lacetonate; NIT-4py = 2-(4-pyridyl)-4, 4, 5, 5-tetramethylimidazoline-1-oxyl-3-oxide; HL^{29} = 8- hydroxyquinoline; H_2L^{30} = 1-[[(2-hydroxyethyl)imino] methyl]-2-naphthalenol; H_2valpn = N, N'-1, 3-propylenebis-3-methoxy-salicylideneamine; 2, 3-HDCB = 2, 3-dichlorobenzoic acid; H_2L^{31} = 4-bromo-2-[(2-hydroxypropylimino)methyl]phenol; dto = dithiooxalate; HL^{32} = [2-(methylsulfanyl)phenyl]salicylaldimine; H_4L^{33} = N, N', N", N"'-tetra(2-hydroxy-3-methoxy-5-methylbenzyl)-1, 4, 7, 10-tetraazacyclododecane; H_2L^{34} = (E)-2-((2-hydroxy-3-methoxybenzylidene)amino)-4-methylphenol; H_2hmmp = 2-[(2-hydroxyethylimino)methyl]-6-methoxyphenol; H_3TTTT^{Me} = 2, 2', 2"-(((nitrilotris-(ethane-2, 1-diyl))tris-(azanediyl))tris(methyl-methylene))tri-phenol; 2, 5-HDCB = 2, 5-dichlorobenzoic acid; phen = 1, 10-phenanthroline

2.1. $[Dy_2Ni_2]$型单分子磁体

近年来，随着人们不断深入研究稀土金属配合物，镧系金属与有机配体形成的配合物引起了越来越多研究者的关注。2014 年，郑智敏领导的研究小组用 Ni^{II}取代了配合物 $Dy_2Co_2(L^1)_{10}(bipy)_2$ 中的 Co^{II}，得到了一个接近等结构的配合物，$Dy_2Ni_2(L^1)_{10}(bipy)_2$(**1**) [23]。相较于其他配合物而言，所得配合物 **1** 结构简单。交流磁化率研究表明，**1** 在零场下也表现出 SMM 行为，有效能势垒为 105(1) K (如图 1)。利用

Arrhenius 定律对数据进行分析表明，在 **1** 研究中至少存在两个松弛过程。高温过程可能与单个 Dy^{III}的自旋轨道态的弛豫有关。通过第一原理计算，发现配合物{Dy_2Co_2}和 **1** 中 Dy^{III}的第一个激发态 Kramers 双态分别为 66 和 61 cm^{-1}，与实验测量的磁反转势垒一致。低温过程可能与交换状态的逆转有关。第一原理计算表明，**1** 中交换型的低能势垒约为 8 cm^{-1}，而在复合物 **27** 中，只有在温度低于 1 K 时才能观察到交换型的反转势垒。因此可以推断，配合物 **27** 和 **1** 的弛豫过程主要是由 Dy^{III}离子的强各向异性控制的，它们的弛豫机制的差异可能归因于过渡金属的变化。

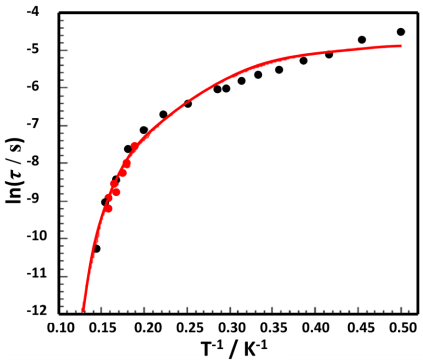

Figure 1. lnτ versus T^{-1} plots for **1** under zero dc field. The red points have been obtained from the ac susceptibility measurements. The black points have been obtained from the fit of the Cole−Cole plots. The red line is obtained by a least-squares fit.
图 1. **1** 在零直流场下的 lnτ 与 T^{-1} 图。红点是由交流磁化率测量得到的。黑点是通过对 Cole−Cole 图的拟合得到的。红线是利用最小二乘拟合得到

2015 年，唐金魁的课题组成功合成了另一种含有 Ni^{II}的三核 3d-4f 单分子磁体，标记为 [$Dy^{III}_2Ni^{II}(C_7H_5O_2)_8$]·($C_7H_6O_2$)$_2$(**2**) [24]。该配合物的核心结构与配合物[$Ln_2Co^{II}(C_7H_5O_2)_8$]·$6H_2O$ (Ln=Dy (**28**), Tb (**29**))基本相同，保持了 Dy-Ni-Dy 的线性排列。此外，**2** 的离子中 Dy^{III}和 Ni^{II}离子的配位环境与配合物 **28**-**29** 中的配位环境相同。交流磁化率测量证实了 **2** 在 1.5 kOe 的外场下的 SMM 行为。值得注意的是，与零场条件下的情况相比，与频率相关的非相交流磁化率的峰值向较低的频率移动。在 ln (τ)和 T^{-1}图中，在 5 K 处的明显交叉表明在 **2** 的图中存在双弛豫过程，与配合物 **1** 类似。利用 Arrhenius 定律拟合数据，确定低温有效势垒为 12.24 K，高温有效有效势垒为 55.19 K (图 2)，高低温的有效势垒相差不大。这两种高、低温弛豫机制可能与 Dy^{III}的单离子行为和 Dy^{III}与 Ni^{II}离子之间的弱耦合相互作用有关。

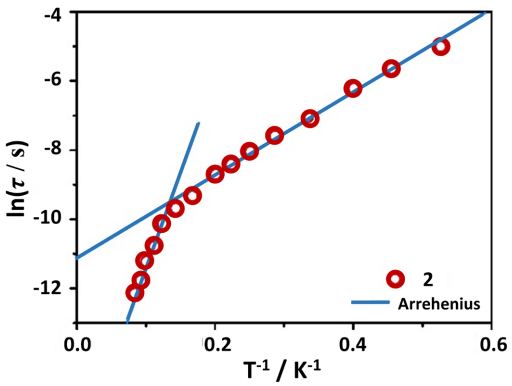

Figure 2. Magnetization relaxation time, ln(τ) *vs* T^{-1} plot for **2** under 1500 Oe. The solid lines are fitted with the Arrhenius law
图 2. 1500 Oe 下 **2** 的磁化弛豫时间，ln(τ) *vs* T^{-1} 图。实线符合 Arrhenius 定律

2016 年，赵小军、刘育[25]等人发现了三个线性{Dy_2Ni_2}团簇，即[$Dy_2Ni_2(bipy)_2(RC_6H_4COO)_{10}$](R = H(**3**)、甲基(**4**)和二氧化氮(**5**))，它们表现出结构相似性。和上述的配合物相比，该类型的配合物结构组成较为复杂。以 **3** 为例，两个中央对称 Dy^{III}离子聚集在一起的两对羧酸同 μ:η^1:η^1 和 μ:η^2:η^1 绑定模式，导致 Dy^{III}协调八羧酸氧原子从七个苯甲酸阴离子，形成一个稍微扭曲的三角形十二面体。随后，{Dy_2}二聚体通过三对羧酸基进一步连接到两个具有八面体配位环境的 Ni^{II}离子上，形成一个线性核心(如图 3(a))。交流磁化率测量显示，配合物 **3** 和 **4** 在零场有明显的峰，表明存在 SMM 的行为。将数据拟合到一个公式中，得到 **3** 和 **4** 的有效能垒分别为 57.06 K 和 37.04 K (如图 3(b))。在 4.6 kOe 的外场作用下，**4** 的有效能势垒增加到 77.08 K，表明 QTM 被有效抑制。然而，对于配合物 **3**，5.8 kOe 的应用场几乎没有改变其有效能垒。相比之下，配合物 **5** 在零场和 10 K 以下的非相交流磁化率中表现出频率依赖的行为，没有可见峰。低温下失相信号的显著增加进一步证实了 QTM 过程在 **5** 中逐渐占主导地位。此外，配合物 **3-5** 中没有一个表现出迟滞环。理论计算表明，选择配合物 **3-5**R 组(−H，$-CH_3$ 或$-NO_2$)可以通过感应或共轭效应改变羧酸氧供体的电荷分布，从而影响基态和第一激发态 Dy^{III}和磁易轴的方向，进一步影响分子各向异性和偶极相互作用。因此，局部配位球内的电荷分布对影响 SMMs 的性能起着关键作用。

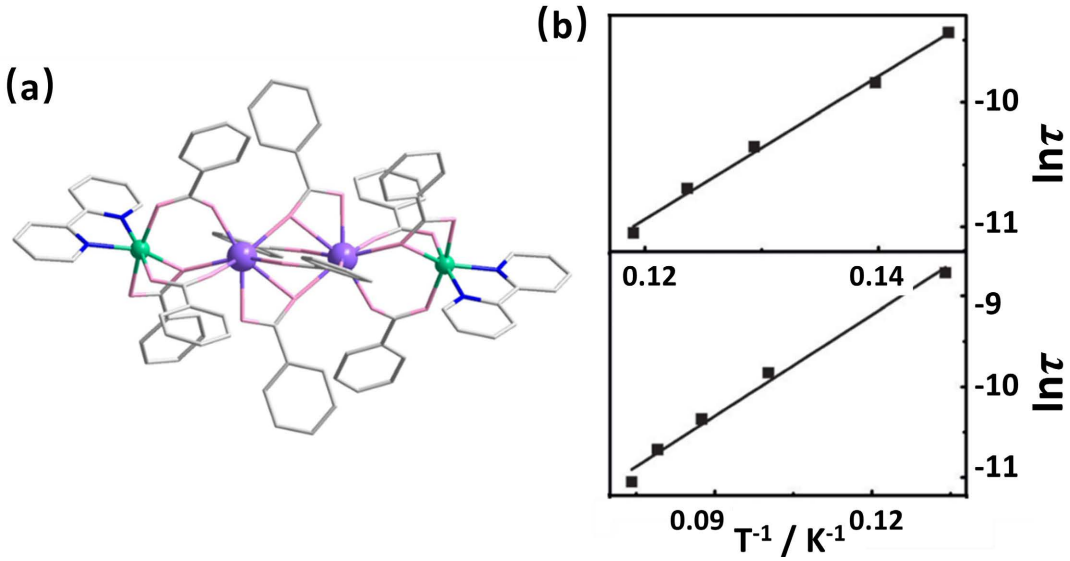

Figure 3. The molecular structure of **3** (a) and plots of ln(τ) vs T^{-1} for **3** (top) and **4** (bottom) under zero dc field (b). The solid lines represent fits to the Arrhenius law for **3** and **4**. Color code: NiII, green; Dy, purple; O, pink; N, blue; C, gray. H atoms are omitted for clarity

图 3. 在零直流场(b).下，**3** (上)和 **4** (下) (a)的分子结构和 ln (τ)与 T^{-1} 的图实线表示符合 **3** 和 **4** 的 Arrhenius 定律。颜色编码：Ni^{II}、绿色；Dy、紫色；O、粉红色；N、蓝色；C、灰色。为了清晰起见，省略了 H 原子

2.2. 缺陷 Dicubane 型单分子磁体

2011 年，Powell 研究小组[26]报告了两对具有缺陷双元(或蝴蝶型)核心拓扑的配合物，分别为[$Ni_2Ln_2(L^{58})_4(NO_3)_2(DMF)_2$] ($H_2L^{58}$ = (E)-2-(2-Hydroxy-3-methoxybenzylideneamino)phenol, Ln = Dy (**6**, Tb (**7**))和[$Ni_2Ln_2(L^{58})_4(NO_3)_2(MeOH)_2$]·3MeOH (Ln = Dy (**8**), Tb (**9**))。在结构上，配合物 **6-9** 是等结构的，唯一的区别是在配合物 **6** 和 **7** 中，与 Ni^{II}离子配位的 DMF 被 MeOH 分子取代。在配合物 **6** 中，两个 Ni^{II}离子占据了与蝴蝶身体相对应的位置，而两个 Dy^{III}离子则位于翅膀的位置(图 4(a))。两个对称的 H_2L^2 配体采用 μ_3:η^1:η^2:η^1:η^2 配位模式，连接外围的 Dy^{III}和 Ni^{II}离子。另外两个 H_2L^2 配体采用 μ_3:η^0:η^1:η^1:η^3 配位模式，连接两个 Ni_2Dy 三角形(图 4(b))。此外，DMF 和硝酸盐离子与 Ni^{II}和 Dy^{III}离子配位，导致 Ni^{II}的八面体构

型略有扭曲，而 Dy^{III}为扭曲的四方反棱柱构型。在零直流场下对所有四种配合物进行了交流磁化率测量。配合物 **6** 和 **8** 表现出较强的频率依赖性的同相和异相信号，**6** 和 **8** 的有效能势垒分别为 18.5 K 和 21.3 K。通过施加 4 kOe 的外磁场，**8** 有效抑制了 QTM 效应的存在，使有效能垒增加到 28.5 K (图 5)。此外，**9** 在 6 K 以下表现出弱频率依赖的虚部信号，**7** 在 1.8 K 以上没有表现出任何频率依赖的虚部信号。因此，综合考虑配合物 **6-9**，Ln^{III}离子的各向异性成为发展 SMM 性能的关键决定因素，这与我们从配合物 **1** 和 **27** 所得出的结论基本一致，可见[Dy_2Ni_2]型单分子磁体和缺陷 Dicubane 型单分子磁体在性质上有某些相同之处。此外，甲醇的能垒 **8** 高于 DMF 的 **6**，表明 Ni^{II}上的配位取代可能显著影响 Ln^{III}各向异性张量的取向和大小。

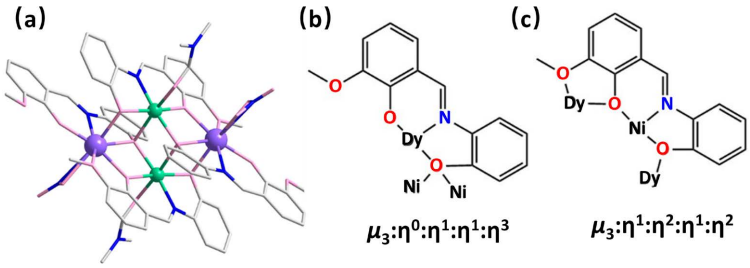

Figure 4. The molecular structure of **6** (a) and the coordination modes of $(L^2)^{2-}$ with metals in complexes **6-9** (b). Color code: Ni^{II}, green; Dy, purple; O, pink; N, blue; C, gray. H atoms are omitted for clarity.
图 4. **6** (a)的分子结构和配合物 **6-9** (b).中的((a)) 2-与金属的配位模式。颜色编码：Ni^{II}，绿色；Dy，紫色；O，粉红色；N、蓝色；C、灰色。为了清晰起见，省略了 H 原子

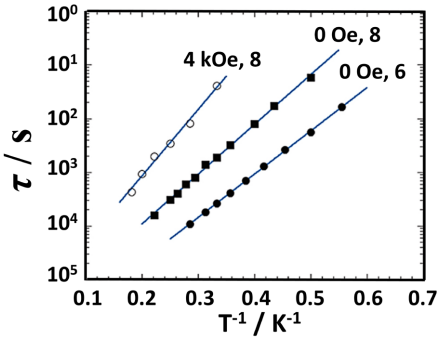

Figure 5. Arrhenius semi-log plots of the relaxation time, τ *vs* 1/*T* of complexes **6** and **8** from ac susceptibility measurements both under zero and an applied dc field of 4000 Oe. The solid lines correspond to a linear fit in the thermally activated range of temperatures.
图 5. 在 0 和 4000 Oe 的直流场下，配合物 **6** 和 **8** 的交流磁化率测量的弛豫时间 τ 与 1/*T* 的 Arrhenius 半对数图。实线对应于热激活温度范围内的线性拟合

2014 年，唐金魁领导的研究团队[27]成功合成了 5 个缺陷六核配合物，是目前核数最多的配合物，分别为[$Ln_2Ni_4(L^3)_2Cl_2(OH)_2(CH_3O)_2(CH_3OH)_6$] (Ln = Gd (**10**), Tb (**11**), Dy (**12**)), and [$Ln_2Ni_4(L^3)_2Cl_2(OH)_4(CH_3OH)_6$] (Ln = Ho (**13**), Y (**14**))。配合物 **10-14** 表现出显著的结构相似性。以配合物 **12** 为例，其核心由两个羟基和两个苯氧基氧原子组成，连接两个缺陷二元单元[Ni_2DyO_3Cl]。每个[Ni_2DyO_3Cl]单元是由连接两个 Ni^{II}离子和一个 Dy^{III}离子通过一个苯氧基，一个羟基，一个甲醇分子，一个氯离子，导致 Dy^{III}采用扭曲的四方反棱柱构型，而 Ni^{II}离子表现出扭曲的八面体构型(图 6)。在零磁场下，**11** 和 **12** 表现出较强的温度和频率相关的同相和非相交流磁化率信号，具有峰值，表明它们的 SMM 行为。复合物 **13** 在 6 K 以下仅显示出微弱的频率相关的交流信号，即使在 2 kOe 的外部磁场下，也没有可观测到的峰值。**10** 和 **14** 在 1.8 K

以上和零外场下没有显示任何虚部磁化率信号。对 **11** 和 **12** 的磁性行为的分析表明，它们的弛豫过程可能遵循热激活机制。用 Arrhenius 定律拟合，得到 **11** 和 **12** 的有效能垒分别为 30 K 和 32 K。虽然配合物 **6** 和 **8** 也表现出了较强的频率依赖性的实部和虚部信号，但有效能垒是 **11** 和 **12** 的一半。此外，**11** 和 **13** 代表了 Ni-Tb 和 Ni-Ho 配合物的第一个实例，在零外场下观察到虚部交流磁化率信号。

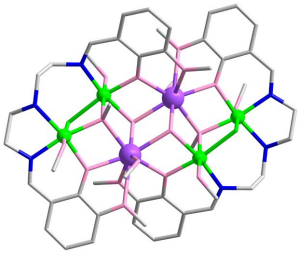

Figure 6. The molecular structure of **12**. Color code: Ni^{II}, green; Dy, purple; O, pink; N, blue; C, gray. H atoms are omitted for clarity
图 6. **12** 的分子结构。颜色编码：Ni^{II}，绿色；Dy，紫色；O，粉红色；N、蓝色；C、灰色。为了清晰起见，省略了 H 原子

2015 年，Fu-Pei Liang 等人[28]使用两种不同的多齿席夫碱配体合成了三个蝴蝶型拓扑的 SMM：$[Dy_2Ni_2(H_2L^5)_2(\mu_3\text{-}OMe)_2(CH_3CN)_2(NO_3)_4]\cdot 4H_2O$ (**15**, H_4L^5 = 2-(((2-hydroxy-3-methoxyphenyl)methylene) amino)-2-(hydroxymethyl)-1, 3-propanedio), $[Ln_2Ni_2(HL^4)_2(\mu_3\text{-}OMe)_2(CH_3CN)_2(NO_3)_4]\cdot 4H_2O$ (Ln = Tb (**16**), Dy (**17**)) (图 7(a))。磁分析显示，三种配合物在直流磁化率方面均表现出强铁磁耦合，在交流磁化率研究中表现出典型的 SMM 行为，各向异性势垒分别为 48.2 K、86.2 K 和 56.6 K (图 7(b))。此外，这三个复合物均表现出狭窄的滞后环。结合理论计算的结果，很明显，Dy^{III}和 Tb^{III}离子具有更高的轴向各向异性，在这些具有蝴蝶型磁滞的配合物中，Ln^{III}离子和 3d 金属离子之间的交换耦合可能明显弱于 Ln^{III}-Ln^{III}的交换作用。这一结论再次验证了 Powell 研究小组的研究结论的正确性。

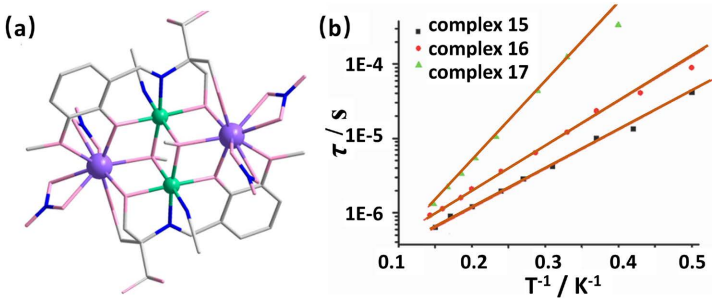

Figure 7. The molecular structure of **15** (a) and Arrhenius semi-log plots of the relaxation time *vs*. 1/T of complexes **15-17** (b). The solid lines correspond to a linear fit in the thermally activated range of temperatures. Color code: Ni^{II}, green; Dy, purple; O, pink; N, blue; C, gray. H atoms are omitted for clarity
图 7. **15** (a) 和阿伦尼乌斯与 **15-17** (b). 弛豫时间的半对数图实线对应于热激活温度范围内的线性拟合。颜色编码：Ni^{II}、绿色、Dy、紫色、O、粉红色、N、蓝色、C、灰色。为了清晰起见，省略了 H 原子

2.3. 其他类型的单分子磁体

2013 年，Vadapalli Chandrasekhar 及其同事[29]合成了 4 个等结构的五核 SMM，记为$\{Ni_2Ln_3\}$ (Ln = Dy (**18**), Gd (**19**), Tb (**20**), Ho (**21**))。配合物 **18** 和 **19** 包括 4 个三层去质子配体$(HL^{6})^{3-}$，其中两个位于配合物的末端，其余两个位于配合物的中心。**18** 和 **19** 的核心由两个末端四核单元$[NiDyO_2]$和两个四元环$[Dy_2O_2]$

组成，它们是相互连接的(图 8(a))。配合物 **20** 和 **21** 本质上与 **18** 和 **19** 是同结构的，唯一的区别是在配合物 **20** 和 **21** 中，中心配体上的一个苯氧原子仍然保持质子化，形成一个双脱质子配体$(HL^6)^{2-}$，而其余三个配体仍然保持三重脱质子$(HL^6)^{3-}$。在直流磁化率测量中，**18** 表现出铁磁基态，而 **19-21** 表现出反铁磁基态。交流磁化率测量显示，**18** 表现出具有两个热激活弛豫过程的 SMM 行为，与上述的 **11** 和 **12** 相似。在 10~17 K 的温度范围内，高温有效能垒为 85 K，τ_0 值为 5.9×10^{-7} s。当温度降至低于 7 K 时，低温有效势垒为 53.5 K。在超过 50 mT/s 的扫描速率下，**18** 的磁滞回线的开放温度高达 3 K，为其单分子磁体行为提供了证据(图 8(b))

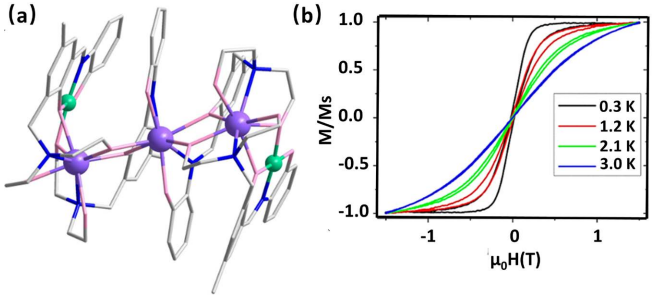

Figure 8. The molecular structure (a) and magnetic hysteresis (b) of complex **18**. Color code: Ni^{II}, green; Dy^{III}, purple; O, pink; N, blue; C, gray. H atoms are omitted for clarity
图 8. 配合物 **18** 的分子结构(a)和磁滞(b)。颜色编码：Ni^{II}，绿色；Dy^{III}，紫色；O，粉红色；N、蓝色；C、灰色。为了清晰起见，省略了 H 原子

2015 年，Constantinos J. Milios 和同事[30]合成了三个笼状配位配合物，$\{Ni_6Ln_3\}$ (Ln=Gd (**22**), Dy (**23**), Er (**24**))。配合物 **22** 和 **24** 是等结构的，而配合物 **23** 由于存在不同的共结晶溶剂分子而有所不同。以配合物 **24** 为例，它包括一个$[Er^{III}_3]$三角形，覆盖着一个$[Ni^{II}_6]$三角棱镜。$[Er^{III}_3]$三角形由 6 个 μ_3-OH 基团锚定，每个 μ_3-OH 部分连接两个 Er^{III}离子和一个 Ni^{II}离子。$[Ni^{II}_6]$三角棱镜包含 6 个 μ_3-O_R 烷基，这 6 个来自 6 个双去质子配体$(HL^7)^{2-}$(H_3L^7 = 2-(*β*-naphthalideneamino)-2-hydroxymethyl-1-propanol)，三角棱镜角的 3 对$[Ni_2]$单元由 μ:η^1:η^1 硝酸基桥接(图 9(a))。为了研究 **22-24** 团簇在零场条件下的磁性能，进行了交流磁化率测量。值得注意的是，只有 **23** 表现出 SMM 的特征，在 3.6 K 以下，虚部信号存在明显的峰(图 9(b))，拟合数据得到 23.84 K 的有效能垒，τ_0 为 3.63×10^{-8} s 。

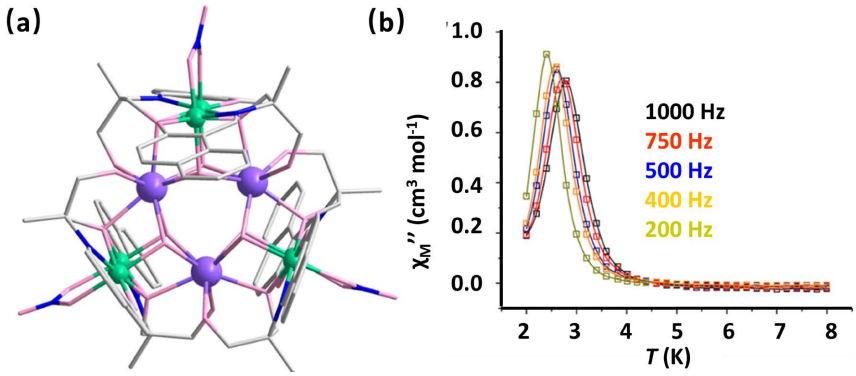

Figure 9. The molecular structure of **15** (a) and plot of χ_M" *vs T* for complex **15** (b). Color code: Ni^{II}, green; Dy^{III}, purple; O, pink; N, blue; C, gray. H atoms are omitted for clarity
图 9. 15 (a)的分子结构和配合物 **15** (b)的 χ_M"与 *T* 的曲线。图颜色编码：Ni^{II}，绿色；Dy^{III}，紫色；O，粉红色；N、蓝色；C、灰色。为了清晰起见，省略了 H 原子

2021 年，童明良领导的研究小组[31]采用对称组装策略和金属生长方法合成了配合物[$Ho^{III}Ni^{II}_5$(quinha)$_5F_2$(dfpy)$_{10}$](**25**, H_2quinha = quinaldichydroxamic acid, dfpy = 3, 5-difluoropyridine)。在配合物 **25** 中，Ho^{III}位于[15-MCNi-5]环内，其中 Ho^{III}与赤道平面上的 5 个氢化氧原子和两个轴向 F^-配位，为 D_{5h}配位环境。5 个四齿醌配体通过 μ_3:η^2:η^1:η^1:η^1 配位模式与 5 个 Ni^{II}离子连接，形成[15-MCNi-5]环。在 0~2 kOe 范围内的外磁场作用下，**25** 的交流磁化率在 50 K 时达到峰值。随着直流场的增加，峰值对应的频率发生变化，但变化的幅度逐渐减小。在高温区域，外磁场对有效能垒的影响可以忽略不计，U_{eff} 为 825.1 K，τ_0(1)，范围为 3.3 (5)~3.6 (6) × 10^{-13} s，是目前发现的所有单分子磁体中有效能垒最大的。这表明，在高温条件下的弛豫过程是由一个单一的 Ho^{III}离子主导的。此外，理论计算结果表明，Ho^{III}的基态与第二激发态之间的能隙接近于 825.1 K 的能垒。在低温区域，能垒随外加磁场的变化而振荡，范围为 26.6 (1)至 32.7 (6) K，τ_0 (2)范围为 5.7 (1) × 10^{-4} 至 9.4 (2) × 10^{-4} s。这些振荡可能来自于在简单单核复合体领域之外发生的超精细状态的塞曼交叉和反移动现象。这些交叉/反移动现象产生了不同的势垒，要么由超精细能级之间的非相干 QTM 主导，要么由涉及激发电子交换双态的类 Orbach 过程主导。综上所述，这一现象是由于各向异性金属离子的强超精细相互作用及其与相邻金属离子的交换耦合引起的。

3. 结论

Ni^{II}在一般配位场下具有由较大的零场分裂导致的高的磁各向异性，其分子配位结构简单，这些特点引起了人们的兴趣，并提出了进一步的综合努力应该关注的方向。通过研究总结 Ni-Ln 单分子磁体的最新研究进展，我们发现影响 SMM 性能的几个重要因素，如 Ln^{III}离子的各向异性、Ni 与 Ln 间耦合相互作用力、Ni 离子周围配位环境及电荷分布等等，为我们后续继续研究 Ni-Ln 单分子磁体提供了指导方向。

但显然，我们对单分子磁体的了解还远不够，有关 Ni-Ln 单分子磁体的研究报告没有非常全面，并且大部分 Ni-Ln 配合物在奥巴赫、拉曼、量子隧穿这些弛豫过程中的参数(U_{eff}、τ_0、QTM)普遍是利用理性数据拟合所得，并非确切真实数据，其可靠度需要评估。由于 Ni^{II}离子复杂而敏感的磁结构，使其磁学性质不稳定，因此目前大部分有关 Ni-Ln 的研究主要集中在磁体的磁学行为及性质、合成和制备技术这些方面。虽然已取得了一些重要的进展，但仍面临着磁构关系不明朗、磁性行为理解片面、合成方法不成熟，工业化生产困难、研究方向单一等问题。这些问题有不少还处于基础研究的阶段，如果可以得到解决，相信对单分子磁体的应用会有更好的指导意义

基金项目

江苏省研究生科研与实践创新计划项目(KYCX24_3546、SJCX24_1995、SJCX24_1992)资助，南通大学大型仪器开放基金资助(KFJN2471、KFJN2437)，感谢南通大学分析测试中心。

参考文献

[1] 苏丹. 稀土基单分子磁体的磁性与多铁性研究[D]: [硕士学位论文]. 北京: 中国科学院大学(中国科学院物理研究所), 2024.

[2] Bogani, L. and Wernsdorfer, W. (2008) Molecular Spintronics Using Single-Molecule Magnets. *Nature Materials*, **7**, 179-186. https://doi.org/10.1038/nmat2133

[3] Affronte, M., Troiani, F., Ghirri, A., Candini, A., Evangelisti, M., Corradini, V., *et al*. (2007) Single Molecule Magnets for Quantum Computation. *Journal of Physics D*: *Applied Physics*, **40**, 2999-3004. https://doi.org/10.1088/0022-3727/40/10/s01

[4] Awschalom, D.D. and DiVincenzo, D.P. (1995) Complex Dynamics of Mesoscopic Magnets. *Physics Today*, **48**, 43-48. https://doi.org/10.1063/1.881448

[5] Sessoli, R., Gatteschi, D., Caneschi, A. and Novak, M.A. (1993) Magnetic Bistability in a Metal-Ion Cluster. *Nature*, **365**, 141-143. https://doi.org/10.1038/365141a0

[6] Murugesu, M., Habrych, M., Wernsdorfer, W., Abboud, K.A. and Christou, G. (2004) Single-Molecule Magnets: A Mn_{25} Complex with a Record *s* = 51/2 Spin for a Molecular Species. *Journal of the American Chemical Society*, **126**, 4766-4767. https://doi.org/10.1021/ja0316824

[7] Murugesu, M., Takahashi, S., Wilson, A., Abboud, K.A., Wernsdorfer, W., Hill, S., *et al*. (2008) Large Mn_{25} Single-Molecule Magnet with Spin *s* = 51/2: Magnetic and High-Frequency Electron Paramagnetic Resonance Spectroscopic Characterization of a Giant Spin State. *Inorganic Chemistry*, **47**, 9459-9470. https://doi.org/10.1021/ic801142p

[8] Tasiopoulos, A.J., Vinslava, A., Wernsdorfer, W., Abboud, K.A. and Christou, G. (2004) Giant Single-Molecule Magnets: A $\{Mn_{84}\}$ Torus and Its Supramolecular Nanotubes. *Angewandte Chemie International Edition*, **116**, 2169-2173. https://doi.org/10.1002/ange.200353352

[9] Milios, C.J., Vinslava, A., Wernsdorfer, W., *et al*. (2007) A Record Anisotropy Barrier for a Single-Molecule Magnet. *Journal of the American Chemical Society*, **129**, 2754-2755.

[10] Costes, J., Dahan, F., Dupuis, A. and Laurent, J. (1996) A Genuine Example of a Discrete Bimetallic (Cu, Gd) Complex: Structural Determination and Magnetic Properties. *Inorganic Chemistry*, **35**, 2400-2402. https://doi.org/10.1021/ic951382q

[11] Bencini, A., Benelli, C., Caneschi, A., Carlin, R.L., Dei, A. and Gatteschi, D. (1985) Crystal and Molecular Structure of and Magnetic Coupling in Two Complexes Containing Gadolinium(III) and Copper(II) Ions. *Journal of the American Chemical Society*, **107**, 8128-8136. https://doi.org/10.1021/ja00312a054

[12] Costes, J., Dahan, F., Dupuis, A. and Laurent, J. (1997) Experimental Evidence of a Ferromagnetic Ground State (*s* = 9/2) for a Dinuclear Gd(III)-Ni(II) Complex. *Inorganic Chemistry*, **36**, 4284-4286. https://doi.org/10.1021/ic970720f

[13] Stemmler, A.J., Kampf, J.W., Kirk, M.L., Atasi, B.H. and Pecoraro, V.L. (1999) The Preparation, Characterization, and Magnetism of Copper 15-Metallacrown-5 Lanthanide Complexes. *Inorganic Chemistry*, **38**, 2807-2817. https://doi.org/10.1021/ic9800233

[14] Liu, J., Chen, Y., Zheng, Y., Lin, W., Ungur, L., Wernsdorfer, W., *et al*. (2013) Switching the Anisotropy Barrier of a Single-Ion Magnet by Symmetry Change from Quasi-D5h to Quasi-oh. *Chemical Science*, **4**, 3310-3316. https://doi.org/10.1039/c3sc50843a

[15] Chen, Y., Liu, J., Ungur, L., Liu, J., Li, Q., Wang, L., *et al*. (2016) Symmetry-Supported Magnetic Blocking at 20 K in Pentagonal Bipyramidal Dy(III) Single-Ion Magnets. *Journal of the American Chemical Society*, **138**, 2829-2837. https://doi.org/10.1021/jacs.5b13584

[16] Canaj, A.B., Dey, S., Martí, E.R., Wilson, C., Rajaraman, G. and Murrie, M. (2019) Insight into D_{6h} Symmetry: Targeting Strong Axiality in Stable Dysprosium(III) Hexagonal Bipyramidal Single-Ion Magnets. *Angewandte Chemie International Edition*, **58**, 14146-14151. https://doi.org/10.1002/anie.201907686

[17] Wen, H., Liu, S., Xie, X., Bao, J., Liu, C. and Chen, J. (2015) A Family of Nickel-Lanthanide Heterometallic Dinuclear Complexes Derived from a Chiral Schiff-Base Ligand Exhibiting Single-Molecule Magnet Behaviors. *Inorganica Chimica Acta*, **435**, 274-282. https://doi.org/10.1016/j.ica.2015.07.009

[18] Li, Z., Li, X., Yan, Y., Hou, L., Zhang, W. and Wang, Y. (2018) Tunable Emission and Selective Luminescence Sensing in a Series of Lanthanide Metal-Organic Frameworks with Uncoordinated Lewis Basic Triazolyl Sites. *Crystal Growth & Design*, **18**, 2031-2039. https://doi.org/10.1021/acs.cgd.7b01453

[19] Zhong, L., Chen, W., Li, X., OuYang, Z., Yang, M., Zhang, Y., *et al*. (2020) Four Dinuclear and One-Dimensional-Chain Dysprosium and Terbium Complexes Based on 2-Hydroxy-3-Methoxybenzoic Acid: Structures, Fluorescence, Single-Molecule-Magnet, and *Ab Initio* Investigation. *Inorganic Chemistry*, **59**, 4414-4423. https://doi.org/10.1021/acs.inorgchem.9b03555

[20] Yu, Y., Pan, X., Cui, C., Luo, X., Li, N., Mei, H., *et al*. (2020) A Series Three-Dimensional Ln_4Cr_4 (Ln = Gd, Tb, Er) Heterometallic Cluster-Based Coordination Polymers Containing Interesting Nanotubes Exhibiting High Magnetic Entropy. *Inorganic Chemistry*, **59**, 5593-5599. https://doi.org/10.1021/acs.inorgchem.0c00281

[21] Wen, H., Hu, J., Yang, K., Zhang, J., Liu, S., Liao, J., *et al*. (2020) Family of Chiral Zn^{II}-Ln^{III} (Ln = Dy and Tb) Heterometallic Complexes Derived from the Amine-Phenol Ligand Showing Multifunctional Properties. *Inorganic Chemistry*, **59**, 2811-2824. https://doi.org/10.1021/acs.inorgchem.9b03164

[22] Tian, Y., Stroppa, A., Chai, Y., Barone, P., Perez-Mato, M., Picozzi, S., *et al*. (2014) High-Temperature Ferroelectricity and Strong Magnetoelectric Effects in a Hybrid Organic-Inorganic Perovskite Framework. *Physica Status Solidi* (*RRL*)—*Rapid Research Letters*, **9**, 62-67. https://doi.org/10.1002/pssr.201409470

[23] Zhao, F.H., Li, H., Che, Y.X., Zheng, J.M., Vieru, V., Chibotaru, L.F., Grandjean, F. and Long, G.J. (2014) Synthesis, Structure, and Magnetic Properties of $Dy_2Co_2L_{10}(bipy)_2$ and $Ln_2Ni_2L_{10}(bipy)_2$, Ln = La, Gd, Tb, Dy, and Ho: Slow Magnetic Relaxation in $Dy_2Co_2L_{10}(bipy)_2$ and $Dy_2Ni_2L_{10}(bipy)_2$. *Inorganic Chemistry*, **53**, 9785-9799.

[24] Li, X., Min, F., Wang, C., Lin, S., Liu, Z. and Tang, J. (2015) Utilizing 3d-4f Magnetic Interaction to Slow the Magnetic Relaxation of Heterometallic Complexes. *Inorganic Chemistry*, **54**, 4337-4344.

https://doi.org/10.1021/acs.inorgchem.5b00019

[25] Li, Y., Shang, Q., Zhang, Y., Yang, E. and Zhao, X. (2016) Fine Tuning of the Anisotropy Barrier by Ligand Substitution Observed in Linear {Dy_2Ni_2} Clusters. *Chemistry—A European Journal*, **22**, 18840-18849. https://doi.org/10.1002/chem.201603800

[26] Mondal, K.C., Kostakis, G.E., Lan, Y., Wernsdorfer, W., Anson, C.E. and Powell, A.K. (2011) Defect-Dicubane Ni_2Ln_2 (Ln = Dy, Tb) Single Molecule Magnets. *Inorganic Chemistry*, **50**, 11604-11611. https://doi.org/10.1021/ic2015397

[27] Zhao, L., Wu, J., Ke, H. and Tang, J. (2014) Family of Defect-Dicubane Ni_4Ln_2 (Ln = Gd, Tb, Dy, Ho) and Ni_4Y_2 Complexes: Rare Tb(III) and Ho(III) Examples Showing SMM Behavior. *Inorganic Chemistry*, **53**, 3519-3525. https://doi.org/10.1021/ic402973g

[28] Zou, H., Sheng, L., Liang, F., Chen, Z. and Zhang, Y. (2015) Experimental and Theoretical Investigations of Four 3d-4f Butterfly Single-Molecule Magnets. *Dalton Transactions*, **44**, 18544-18552. https://doi.org/10.1039/c5dt03368c

[29] Chandrasekhar, V., Bag, P., Kroener, W., Gieb, K. and Müller, P. (2013) Pentanuclear Heterometallic {Ni_2Ln_3} (Ln = Gd, Dy, Tb, Ho) Assemblies. Single-Molecule Magnet Behavior and Multistep Relaxation in the Dysprosium Derivative. *Inorganic Chemistry*, **52**, 13078-13086. https://doi.org/10.1021/ic4019025

[30] Canaj, A.B., Tzimopoulos, D.I., Siczek, M., Lis, T., Inglis, R. and Milios, C.J. (2015) Enneanuclear [Ni_6Ln_3] Cages: [Ln^{III}_3] Triangles Capping [Ni^{II}_6] Trigonal Prisms Including a [Ni_6Dy_3] Single-Molecule Magnet. *Inorganic Chemistry*, **54**, 7089-7095. https://doi.org/10.1021/acs.inorgchem.5b01149

[31] Wu, S., Ruan, Z., Huang, G., Zheng, J., Vieru, V., Taran, G., *et al*. (2021) Field-Induced Oscillation of Magnetization Blocking Barrier in a Holmium Metallacrown Single-Molecule Magnet. *Chem*, **7**, 982-992. https://doi.org/10.1016/j.chempr.2020.12.022

[32] Maity, S., Ghosh, T.K., Ito, S., Bhunia, P., Ishida, T. and Ghosh, A. (2022) Structures and Magnetic Properties of Carbonato-Bridged Hexanuclear $Ni^{II}_4Ln^{III}_2$ (Ln = Gd, Tb, Dy) Complexes Formed by Atmospheric Carbon Dioxide Fixation in the Absence of an External Base. *Crystal Growth & Design*, **22**, 4332-4342. https://doi.org/10.1021/acs.cgd.2c00298

[33] Pointillart, F., Bernot, K., Sessoli, R. and Gatteschi, D. (2007) Effects of 3d-4f Magnetic Exchange Interactions on the Dynamics of the Magnetization of Dy^{III}-M^{II}-Dy^{III} Trinuclear Clusters. *Chemistry—A European Journal*, **13**, 1602-1609. https://doi.org/10.1002/chem.200601194

[34] Chandrasekhar, V., Pandian, B.M., Boomishankar, R., Steiner, A., Vittal, J.J., Houri, A., *et al*. (2008) Trinuclear Heterobimetallic Ni_2Ln Complexes [L_2Ni_2Ln][ClO_4] (Ln = La, Ce, Pr, Nd, Sm, Eu, Gd, Tb, Dy, Ho, and Er; Lh_3 = (s)p[n(me)n═Ch-C_6H_3-*2*-Oh-3-Ome]$_3$): From Simple Paramagnetic Complexes to Single-Molecule Magnet Behavior. *Inorganic Chemistry*, **47**, 4918-4929. https://doi.org/10.1021/ic800199x

[35] Sutter, J., Dhers, S., Rajamani, R., Ramasesha, S., Costes, J., Duhayon, C., *et al*. (2009) Hetero-Metallic {3d-4f-5d} Complexes: Preparation and Magnetic Behavior of Trinuclear [(L^{me2}Ni-Ln){w(cn)$_8$}] Compounds (Ln = Gd, Tb, Dy, Ho, Er, Y; L^{me2} = Schiff Base) and Variable SMM Characteristics for the Tb Derivative. *Inorganic Chemistry*, **48**, 5820-5828. https://doi.org/10.1021/ic900003m

[36] Colacio, E., Ruiz-Sanchez, J., White, F.J. and Brechin, E.K. (2011) Strategy for the Rational Design of Asymmetric Triply Bridged Dinuclear 3d-4f Single-Molecule Magnets. *Inorganic Chemistry*, **50**, 7268-7273. https://doi.org/10.1021/ic2008599

[37] Gao, Y., Zhao, L., Xu, X., Xu, G., Guo, Y., Tang, J., *et al*. (2011) Heterometallic Cubanes: Syntheses, Structures, and Magnetic Properties of Lanthanide(III)-Nickel(II) Architectures. *Inorganic Chemistry*, **50**, 1304-1308. https://doi.org/10.1021/ic101849h

[38] Colacio, E., Ruiz, J., Mota, A.J., Palacios, M.A., Cremades, E., Ruiz, E., *et al*. (2012) Family of Carboxylate- and Nitrate-Diphenoxo Triply Bridged Dinuclear $Ni^{II}Ln^{III}$ Complexes (Ln = Eu, Gd, Tb, Ho, Er, Y): Synthesis, Experimental and Theoretical Magneto-Structural Studies, and Single-Molecule Magnet Behavior. *Inorganic Chemistry*, **51**, 5857-5868. https://doi.org/10.1021/ic3004596

[39] Peng, J., Zhang, Q., Kong, X., Zheng, Y., Ren, Y., Long, L., *et al*. (2012) High-Nuclearity 3d-4f Clusters as Enhanced Magnetic Coolers and Molecular Magnets. *Journal of the American Chemical Society*, **134**, 3314-3317. https://doi.org/10.1021/ja209752z

[40] Sakamoto, S., Fujinami, T., Nishi, K., Matsumoto, N., Mochida, N., Ishida, T., Sunatsuki, Y. and Re, N. (2013) Carbonato-Bridged $Ni^{II}_2Ln^{III}_2$ (Ln^{III} = Gd^{III}, $Tb^{III,}$ Dy^{III}) Complexes Generated by Atmospheric CO_2 Fixation and Their Single-Molecule-Magnet Behavior: [(μ_4-CO_3)$_2${Ni^{II}(3-MeOsaltn)(MeOH or H_2O)Ln^{III}(NO_3)}$_2$]·Solvent [3-MeOsaltn = N,N'-Bis(3-methoxy-2-oxybenzylidene)-1,3-propanediaminato]. *Inorganic Chemistry*, **52**, 7218-7229.

[41] Towatari, M., Nishi, K., Fujinami, T., Matsumoto, N., Sunatsuki, Y., Kojima, M., *et al*. (2013) Syntheses, Structures, and

Magnetic Properties of Acetato- and Diphenolato-Bridged 3d-4f Binuclear Complexes [M(3-MeOsaltn)(MeOH)$_x$(ac)Ln(hfac)$_2$] (M = Zn^{II}, Cu^{II}, Ni^{II}, Co^{II}; Ln = La^{III}, Gd^{III}, Tb^{III}, Dy^{III}; 3-MeOsaltn = N,N'-Bis(3-methoxy-2-oxybenzylidene)-1,3-propanediaminato; ac = Acetato; hfac = Hexafluoroacetylacetonato; x = 0 or 1). *Inorganic Chemistry*, **52**, 6160-6178.

[42] Ahmed, N., Das, C., Vaidya, S., Langley, S.K., Murray, K.S. and Shanmugam, M. (2014) Nickel(II)-Lanthanide(III) Magnetic Exchange Coupling Influencing Single-molecule Magnetic Features in {Ni$_2$Ln$_2$} Complexes. *Chemistry—A European Journal*, **20**, 14235-14239. https://doi.org/10.1002/chem.201404393

[43] Goura, J., Guillaume, R., Rivière, E. and Chandrasekhar, V. (2014) Hexanuclear, Heterometallic, Ni$_3$Ln$_3$ Complexes Possessing O-Capped Homo- and Heterometallic Structural Subunits: SMM Behavior of the Dysprosium Analogue. *Inorganic Chemistry*, **53**, 7815-7823. https://doi.org/10.1021/ic403090z

[44] Moreno Pineda, E., Chilton, N.F., Tuna, F., Winpenny, R.E.P. and McInnes, E.J.L. (2015) Systematic Study of a Family of Butterfly-Like {M$_2$Ln$_2$} Molecular Magnets (M = Mg^{II}, Mn^{III}, Co^{II}, Ni^{II}, and Cu^{II}; Ln = Y^{III}, Gd^{III}, Tb^{III}, Dy^{III}, Ho^{III}, and Er^{III}). *Inorganic Chemistry*, **54**, 5930-5941. https://doi.org/10.1021/acs.inorgchem.5b00746

[45] Zhang, S., Li, H., Duan, E., Han, Z., Li, L., Tang, J., *et al*. (2016) A 3D Heterometallic Coordination Polymer Constructed by Trimeric {NiDy$_2$} Single-Molecule Magnet Units. *Inorganic Chemistry*, **55**, 1202-1207. https://doi.org/10.1021/acs.inorgchem.5b02378

[46] Liu, M., Hu, K., Liu, C., Cui, A. and Kou, H. (2017) Metallocyclic Ni$_4$Ln$_2$M$_2$ Single-Molecule Magnets. *Dalton Transactions*, **46**, 6544-6552. https://doi.org/10.1039/c7dt00948h

[47] Wu, H., Li, M., Zhang, S., Ke, H., Zhang, Y., Zhuang, G., *et al*. (2017) Magnetic Interaction Affecting the Zero-Field Single-Molecule Magnet Behaviors in Isomorphic {Ni$^{II}_2$Dy$^{III}_2$} and {Co$^{II}_2$Dy$^{III}_2$} Tetranuclear Complexes. *Inorganic Chemistry*, **56**, 11387-11397. https://doi.org/10.1021/acs.inorgchem.7b01840

[48] Canaj, A.B., Tzimopoulos, D.I., Kalofolias, D.A., Siczek, M., Lis, T., Murrie, M., *et al*. (2018) Heterometallic Lanthanide-Centred [N$^{III}_6$Ln^{III}] Rings. *Dalton Transactions*, **47**, 12863-12867. https://doi.org/10.1039/c8dt02855a

[49] Fan, S., Xu, S., Zheng, X., Yan, Z., Kong, X., Long, L., *et al*. (2018) Four 3d-4f Heterometallic Ln$_{45}$M$_7$ Clusters Protected by Mixed Ligands. *CrystEngComm*, **20**, 2120-2125. https://doi.org/10.1039/c8ce00173a

[50] Mandal, S., Ghosh, S., Takahashi, D., Christou, G. and Mohanta, S. (2018) Single-Crystal to Single-Crystal Transformations and Magnetic Properties of a Series of "Butterfly" Ni$^{II}_2$Ln$^{III}_2$ Compounds: SMM Behavior of the Dysprosium(III) Analogue. *European Journal of Inorganic Chemistry*, **2018**, 2793-2804. https://doi.org/10.1002/ejic.201800359

[51] Pei, S., Hu, Z., Chen, Z., Yu, S., Li, B., Liang, Y., *et al*. (2018) Heterometallic Hexanuclear Ni$_4$M$_2$ (M = Dy, Y) Complexes: Structure and Single-Molecule Magnet for the Dy(III) Derivative. *Dalton Transactions*, **47**, 1801-1807. https://doi.org/10.1039/c7dt04003b

[52] Bhanja, A., Herchel, R., Trávníček, Z. and Ray, D. (2019) Two Types of Hexanuclear Partial Tetracubane [Ni$_4$Ln$_2$] (Ln = Dy, Tb, Ho) Complexes of Thioether-Based Schiff Base Ligands: Synthesis, Structure, and Comparison of Magnetic Properties. *Inorganic Chemistry*, **58**, 12184-12198. https://doi.org/10.1021/acs.inorgchem.9b01517

[53] Ge, J., Chen, Z., Qiu, Y., Huo, D., Zhang, Y., Wang, P., *et al*. (2019) Modulating Magnetic Property of Phthalocyanine Supported M^{II}-Dy^{III} (M = Ni, Zn) Heterodinuclear Complexes. *Inorganic Chemistry*, **58**, 9387-9396. https://doi.org/10.1021/acs.inorgchem.9b01179

[54] Mayans, J., Saez, Q., Font-Bardia, M. and Escuer, A. (2019) Enhancement of Magnetic Relaxation Properties with 3d Diamagnetic Cations in [Zn^{II}Ln^{III}] and [Ni^{II}Ln^{III}], Ln^{III} = Kramers Lanthanides. *Dalton Transactions*, **48**, 641-652. https://doi.org/10.1039/c8dt03679a

[55] Meseguer, C., Palacios, M.A., Mota, A.J., Drahoš, B., Brechin, E.K., Navarrete, R., *et al*. (2019) Effect of Π-Aromatic Spacers on the Magnetic Properties and Slow Relaxation of Double Stranded Metallacyclophanes with a Ln^{III}-M^{II}-M^{II}-Ln^{III} (Ln^{III} = Gd^{III}, Dy^{III}, Y^{III}; M^{II} = N^{III}, Co^{II}) Linear Topology. *Polyhedron*, **170**, 373-387. https://doi.org/10.1016/j.poly.2019.05.054

[56] Zhang, J., Liu, W., Wang, C., Xu, S., Liu, B. and Dong, Y. (2019) Syntheses and Properties of Three Types of 3,4-Dichlorobenzoate-Based Ni(^{II})-Ln(^{III}) Heterometallic Clusters. *ChemistrySelect*, **4**, 12418-12423. https://doi.org/10.1002/slct.201902628

[57] Zhou, H., Dong, R., Wang, Z., Wu, L., Liu, Y. and Shen, X. (2019) The Influence of d-f Coupling on Slow Magnetic Relaxation in Ni^{II}Ln^{III}M^{III} (Ln = Gd, Tb, Dy; M = Cr, Fe, Co) Clusters. *European Journal of Inorganic Chemistry*, **2019**, 2361-2367. https://doi.org/10.1002/ejic.201900263

[58] Bhanja, A., Schulze, M., Herchel, R., Moreno-Pineda, E., Wernsdorfer, W. and Ray, D. (2020) Selective Coordination of Self-Assembled Hexanuclear [Ni$_4$Ln$_2$] and [Ni$_2$Mn$_2$Ln$_2$] (Ln = Dy^{III}, Tb^{III}, and Ho^{III}) Complexes: Stepwise Synthesis, Structures, and Magnetic Properties. *Inorganic Chemistry*, **59**, 17929-17944. https://doi.org/10.1021/acs.inorgchem.0c02148

[59] Maity, S., Ghosh, T.K., Gómez-García, C.J. and Ghosh, A. (2020) Hexanuclear Ni$^{II}_4$Ln$^{III}_2$ Complexes with SMM Be-

havior at Zero Field for Ln = Tb, Dy, Ho. *Crystal Growth & Design*, **20**, 7300-7311. https://doi.org/10.1021/acs.cgd.0c00957

[60] Shukla, P., Roy, S., Dolui, D., Cañón-Mancisidor, W. and Das, S. (2020) Pentanuclear Spirocyclic Ni_4Ln Derivatives: Field Induced Slow Magnetic Relaxation in the Dysprosium and Erbium Analogues. *European Journal of Inorganic Chemistry*, **2020**, 823-832. https://doi.org/10.1002/ejic.201901350

[61] Yang, P., Yu, S., Quan, L., Hu, H., Liu, D., Liang, Y., *et al*. (2020) Structure and Magnetic Properties of Two Discrete 3d-4f Heterometallic Complexes. *ChemistrySelect*, **5**, 9946-9951. https://doi.org/10.1002/slct.202002611

[62] Antkowiak, M., Majee, M.C., Maity, M., Mondal, D., Kaj, M., Lesiów, M., *et al*. (2021) Generalized Heisenberg-Type Magnetic Phenomena in Coordination Polymers with Nickel-Lanthanide Dinuclear Units. *The Journal of Physical Chemistry C*, **125**, 11182-11196. https://doi.org/10.1021/acs.jpcc.1c01947

[63] Wang, X., Han, J., Huang, X. and Li, L. (2021) Ln^{III}-N^{III} Heterometallic Compounds Linked by Nitronyl Nitroxides: Structure and Magnetism. *Inorganic Chemistry Communications*, **134**, Article ID: 108983. https://doi.org/10.1016/j.inoche.2021.108983

[64] Yang, P., Hu, H., Yu, S., Liu, D., Liang, Y., Zou, H., *et al*. (2021) Superb Alkali-Resistant $Dy^{III}_2Ni^{II}_4$ Single-Molecule Magnet. *Inorganic Chemistry*, **60**, 14752-14758. https://doi.org/10.1021/acs.inorgchem.1c01963

[65] Yu, S., Zhang, Q., Chen, Z., Zou, H., Hu, H., Liu, D., *et al*. (2021) Structure, Assembly Mechanism and Magnetic Properties of Heterometallic Dodecanuclear Nanoclusters $Dy^{III}_4M^{II}_8$ (M = Ni, Co). *Inorganic Chemistry Frontiers*, **8**, 5214-5224. https://doi.org/10.1039/d1qi01051d

[66] Zeng, M., Hu, K., Liu, C. and Kou, H. (2021) Heterotrimetallic $Ni_2Ln_2Fe_3$ Chain Complexes Based on $[Fe(1\text{-}Ch_3im)\text{-}(Cn)_5]^{2-}$. *Dalton Transactions*, **50**, 6427-6431. https://doi.org/10.1039/d1dt00693b

[67] Zheng, J., Zhang, Y., Shen, Y., Chen, F., Liu, B. and Zhang, J. (2021) Syntheses and Magnetic Properties of a Series of Discrete Ni(II)-Ln(III) Heterometallic Complexes Based on 2,3-Dichlorobenzoate and 2,2'-Bipyridine. *Polyhedron*, **206**, Article ID: 115328. https://doi.org/10.1016/j.poly.2021.115328

[68] Yu, S., Hu, H., Zou, H., Liu, D., Liang, Y., Liang, F., *et al*. (2022) Two Heterometallic Nanoclusters $[Dy^{III}_4Ni^{II}_8]$ and $[Dy^{III}_{10}Mn^{III}_4Mn^{II}_2]$: Structure, Assembly Mechanism, and Magnetic Properties. *Inorganic Chemistry*, **61**, 3655-3663. https://doi.org/10.1021/acs.inorgchem.1c03768

[69] Alouani-Dahmouni, N.E., Rabelo, R., Mayans, J., Moliner, N., Stiriba, S., Julve, M., *et al*. (2023) Solvatotuning of the Field-Induced Slow Magnetic Relaxation through a Single-Crystal-to-Single-Crystal Transformation in Pentanuclear Gadolinium(III)-Nickel(II) Complexes. *Crystal Growth & Design*, **23**, 5403-5408. https://doi.org/10.1021/acs.cgd.3c00511

[70] Dutta, B., Guizouarn, T., Pointillart, F., Kotrle, K., Herchel, R. and Ray, D. (2023) Lanthanoid Coordination Prompts Unusually Distorted Pseudo-Octahedral Ni^{II} Coordination in Heterodinuclear Ni-Ln Complexes: Synthesis, Structure and Understanding of Magnetic Behaviour through Experiment and Computation. *Dalton Transactions*, **52**, 10402-10414. https://doi.org/10.1039/d3dt01387a

[71] Jing, Y., Wang, J., Kong, M., Wang, G., Zhang, Y. and Song, Y. (2023) Detailed Magnetic Properties and Theoretical Calculation in Ferromagnetic Coupling Dy^{III}-M^{II} 3d-4f Complexes Based on a 1,4,7,10-Tetraazacyclododecane Derivative. *Inorganica Chimica Acta*, **546**, Article ID: 121301. https://doi.org/10.1016/j.ica.2022.121301

[72] Li, G., Tang, H., Gao, R., Wang, Y., Sun, X. and Zhang, K. (2023) Tuning Quantum Tunneling in Isomorphic $\{M^{II}_2Dy^{III}_2\}$ "Butterfly" System via 3d-4f Magnetic Interaction. *Crystal Growth & Design*, **23**, 1575-1580. https://doi.org/10.1021/acs.cgd.2c01198

[73] Liu, H., Yu, C., Wang, H. and Pan, Z. (2023) Synthesis, Crystal Structures and Magnetic Properties of Two Ni-Dy Heterometallic Complexes with the Structural Topologies Regulated by Employing Different Schiff Base Ligands. *Polyhedron*, **243**, Article ID: 116566. https://doi.org/10.1016/j.poly.2023.116566

[74] Ruan, Z., Lai, J., Li, J., Zhao, X., Huang, G., Wu, S., *et al*. (2023) Deciphering the Enigma of a Temperature-Dependent Best-Performance Field in Single-Molecule Magnets. *The Journal of Physical Chemistry C*, **127**, 14450-14457. https://doi.org/10.1021/acs.jpcc.3c02541

[75] Shen, Y., Qu, T., Zhang, X., Chen, F., Liu, B. and Zhang, J. (2023) Six Nickel-Lanthanoid Heterometallic Complexes Based on 2,5-Dichlorobenzoate and Phen: Syntheses, Structures and Magnetic Properties. *Inorganica Chimica Acta*, **546**, Article ID: 121295. https://doi.org/10.1016/j.ica.2022.121295